

# The impact of environment on the dynamical structure of satellite systems

A. Faltenbacher <sup>\*</sup>

*Physics Department, University of the Western Cape, Cape Town 7535, South Africa*

*Max-Planck-Institute for Astrophysics, Karl-Schwarzschild-Str. 1, D-85741 Garching, Germany*

*MPA/SHAO Joint Center for Astrophysical Cosmology at Shanghai Astronomical Observatory, Nandan Road 80, Shanghai 200030, China*

13 March 2022

## ABSTRACT

We examine the effects of environment on the dynamical structure of satellite systems based on the Millennium–II Simulation. Satellite halos are defined as sub–halos within the virial radius of a host halo. The satellite sample is restricted to those sub–halos which showed a maximum circular velocity above  $30 \text{ km s}^{-1}$  at the time of accretion. Host halo masses range from  $10^{11}$  to  $10^{14} h^{-1} M_{\odot}$ . We compute the satellites’ average accretion redshift,  $z_{\text{acc}}$ , velocity dispersion,  $\sigma$ , and velocity anisotropy parameter,  $\beta$ , utilising stacked satellite samples of equal mass hosts at similar background densities. The main results are: (1) On average satellites within hosts in high density environments are accreted earlier ( $\Delta z \approx 0.1$ ) compared to their counterparts at low densities. For host masses above  $5 \times 10^{13} h^{-1} M_{\odot}$  this trend weakens and may reverse for higher host masses; (2) The velocity dispersion of satellites in low density environments follows that of the host, i.e. no velocity bias is observed for host halos at low densities independent of host mass. However, for low mass hosts in high density environments the velocity dispersion of the satellites can be up to  $\sim 30\%$  larger than that of the host halo, i.e. the satellites are dynamically hotter than their host halos. (3) The anisotropy parameter depends on host mass and environment. Satellites of massive hosts show more radially biased velocity distributions. Moreover in low density environments satellites have more radially biased velocities ( $\Delta\beta \gtrsim 0.1$ ) compared to their counterparts in high density environments. We believe that our approach allows to predict a similar behaviour for observed satellite galaxy systems.

**Key words:** methods: N-body simulations — methods: numerical — dark matter — galaxies: haloes — galaxies: clusters: general

## 1 INTRODUCTION

The dependence of halo statistics on a second parameter in addition to mass is now generally referred to as assembly bias. Simple extensions to the Press-Schechter and excursion set models (Press & Schechter 1974; Kaiser 1984; Bond et al. 1991; Cole & Kaiser 1989; Lacey & Cole 1993; Mo & White 1996) predict the clustering of halos to depend on their mass alone. However, Gao et al. (2005) and various subsequent studies showed that clustering also depends on other halo properties, for example, formation time, concentration, substructure content, spin and shape (Harker et al. 2006; Wechsler et al. 2006; Bett et al. 2007; Gao & White 2007; Jing et al. 2007; Macciò et al. 2007; Wetzel et al. 2007; Angulo et al. 2008). Using a mass filter in configuration space rather than in k-space Zentner (2007)

demonstrated that excursion set models predict that halos in denser environments do form later, independent of halo mass. At the high mass end this agrees with findings from N-body simulations (e.g., Wechsler et al. 2002; Jing et al. 2007), but is opposite to the behaviour observed at the low mass end. Based on statistics of the peaks within Gaussian random fluctuations, Dalal et al. (2008) argued that the behaviour for low mass halos can be understood if cessation of mass accretion is taken into account. A similar argument has been proposed by Hahn et al. (2009).

Several other studies have investigated the dependence of halo formation times or, similarly, merger rates on environment (e.g., Gottlöber et al. 2001, 2002; Sheth & Tormen 2004; Fakhouri & Ma 2009, 2010; Hahn et al. 2007). Although slightly different density estimators are employed, such as over density in a sphere or mark correlation functions, it is generally agreed upon that halos less massive

<sup>\*</sup> E-mail:afaltenbacher@uwc.ac.za

than  $\sim 10^{13} h^{-1} M_{\odot}$ , which reside in high density regions, form earlier compared to those with equal mass but located in less dense regions.

In a preceding study we discussed the dependence of the dynamical structure of dark matter halos on environment (Faltenbacher & White 2010). We have found that the velocity dispersion of dark matter halos residing in less dense environments shows a more radially biased velocity structure compared to halos of the same mass in denser environments. We now extend this study to the dynamics of satellites within host halos. Satellites are selected on the basis that our findings can be applied to observed satellite galaxy systems. The effects of environment on the dynamical structure of satellites may have important implications for the accretion processes of the host galaxies.

The outline of the paper is as follows. In § 2 we introduce the simulation and the halo finding procedure. We then explain how the environment of host halos is determined and describe the stacking procedure to compute average properties of satellite populations. § 3 presents the results: host halo properties as a function of environment are shown in § 3.1; main results are portrayed in § 3.2 where we discuss the accretion history and dynamical structure of satellite systems. In § 3.3 we investigate resolution effects. A conclusion is given in § 4.

## 2 METHODOLOGY

In this section we describe the tools for our analysis. A short account on the Millennium-II Simulation is followed by the discussion of the halo finding procedure. We also explain the determination of the background density and the stacking procedure used to derive averaged properties of satellite systems in different environments.

### 2.1 Simulation

The Millennium-II Simulation (Boylan-Kolchin et al. 2009; Springel 2005) adopted concordance values for the parameters of a flat  $\Lambda$  cold dark matter ( $\Lambda$ CDM) cosmological model,  $\Omega_m = 0.25$  and  $\Omega_b = 0.045$  for the current matter and baryon densities,  $h = 0.73$  for the present dimensionless value of the Hubble constant,  $\sigma_8 = 0.9$  for the rms linear mass fluctuation in a sphere of radius  $8 h^{-1} \text{Mpc}$  extrapolated to  $z = 0$ , and  $n = 1$  for the slope of the primordial fluctuation spectrum. The simulation followed  $2160^3$  dark matter particles from  $z = 127$  to the present day within a cubic region  $100 h^{-1} \text{Mpc}$  on a side resulting in individual particle masses of  $6.9 \times 10^6 h^{-1} M_{\odot}$ . The gravitational force had a Plummer-equivalent comoving softening of  $1 h^{-1} \text{kpc}$ . We refer readers to Boylan-Kolchin et al. (2009) for more detailed description of the simulation.

### 2.2 Halo sample and accretion times

The halos are found by a two-step procedure. In the first step all collapsed halos with at least 20 particles are identified using a friends-of-friends (fof) group-finder with linking parameter  $b = 0.2$ . These objects will be referred

to as fof-halos. Then post-processing with the substructure algorithm SUBFIND (Springel et al. 2001) subdivides each fof-halo into a set of self-bound sub-halos. Sub-halos with less than 20 particles are discarded. Here we consider the most prominent sub-halo within each fof-halo as host halo. To characterise a host halo we use: the maximal circular velocity,  $V_{\text{max}}$ , which peaks at a radius,  $R_{\text{max}}$ ; the concentration,  $c_{\text{max}} = R_{\text{vir}}/R_{\text{max}}$ , where  $R_{\text{vir}}$  denotes the virial radius, i.e., the radius of a sphere centred at the potential minimum of the host which comprises a mean density of 94 times the critical value. For a Navarro-Frenk-White density profile (Navarro et al. 1997),  $R_{\text{max}}$  is a factor of  $\sim 2.1$  larger than the scale radius  $R_s$ , which has conventionally been used to compute the concentration; and the three dimensional velocity dispersion,  $\sigma_{3\text{DH}}$ , which is based on the velocities of all host halo particles after subtracting their common bulk velocity from each of them. The velocity dispersion of each individual halo,  $\sigma_{3\text{DH}}$ , is scaled its virial velocity  $V_{\text{vir}} = (GM_{\text{vir}}/R_{\text{vir}})^{1/2}$ , where  $M_{\text{vir}}$  is the virial mass and  $G$  is the gravitational constant.

Besides the *host halo*, all other sub-halos with more than 100 particles and located within the virial radius of the host are referred to as *satellite halos*. We only take into account sub-halos within the virial radius of the host halo to prevent the contribution of sub-halos within falsely linked ‘dumbbell’ shaped fof halos. The lower limit of 100 particles is imposed to guarantee a reliable determination of the satellites’ velocities. The accretion redshift of a satellite halo onto the host halo is determined as the redshift at which it discontinues to be the most prominent sub-halo in its own fof-halo. The time elapsing between two consecutive snapshots is roughly 0.3 Gyr which determines the accuracy the accretion times used here. We define the redshift of the snapshot just prior to accretion as *accretion redshift*. This typically corresponds to the time when the halo acquires the maximum mass during the course of its evolution (cf., Guo et al. 2010). With  $V_{\text{max,acc}}$  we denote the maximum circular velocity of the halo at that time. Following Kravtsov et al. (2004) we include only those satellite halos in our analysis with  $V_{\text{max,acc}} \geq 30 \text{ km s}^{-1}$ . This restriction results in a mean of few 1000 simulation particles per arriving satellite. Halos with lower masses presumably contain only negligible amounts of stars. We abandon this requirement only for a resolution study in § 3.3.

### 2.3 The background density field

The background density field is computed based on all sub-halos with maximum circular velocities,  $V_{\text{max}}$ , between  $200 \text{ km s}^{-1}$  and  $300 \text{ km s}^{-1}$ . As Figure 1 illustrates, this velocity range corresponds to halo masses close to  $M_* = 6.15 \times 10^{12} h^{-1} M_{\odot}$  which is the typical collapse mass at  $z = 0$  for the given cosmology. Halos in this mass range provide a relatively unbiased sampling of the overall density field. We denote these halos as  $V_*$ -halos. To facilitate the comparison with density estimates based on observed galaxies we include all sub-halos within the given velocity range irrespective of whether they are host or satellite halos. In total there are 2013  $V_*$  halos resulting in a sampling of the density field based on a point set with

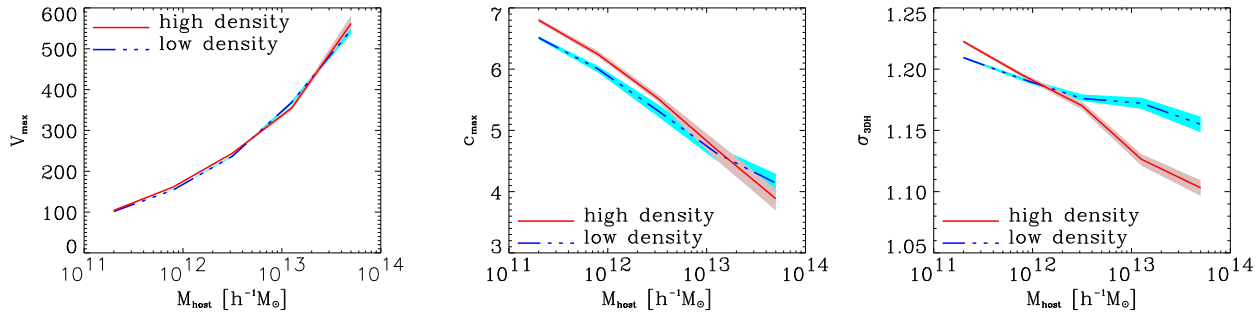


**Figure 1.** Average host halo properties, maximum circular velocity ( $V_{\max}$ ), concentration ( $c_{\max}$ ) and 3D velocity dispersion ( $\sigma_{3\text{DH}}$ ), as a function of halo mass. Red (solid) and blue (dot-dashed) lines display results based on halos in the upper and lower 33% tails of their background density distributions. Halo concentrations,  $c_{\max}$ , are defined as the ratio of the virial mass to the radius of the maximum circular velocity. Before averaging the velocity dispersion of each individual halo is scaled by its virial velocity,  $V_{\text{vir}} = (GM_{\text{vir}}/R_{\text{vir}})^{\frac{1}{2}}$ . The shaded regions indicate the  $1\sigma$  confidence intervals based on a bootstrap resampling.

a mean distance of slightly less than  $8 h^{-1}\text{Mpc}$ .

The background density for any given halo is determined by the seven nearest  $V_*$  halos, each of them smoothed with a smoothing kernel of the form (Monaghan & Lattanzio 1985)

$$W(r; h) = \frac{8}{\pi h^3} \begin{cases} 1 - 6\left(\frac{r}{h}\right)^2 + 6\left(\frac{r}{h}\right)^3, & 0 \leq \frac{r}{h} \leq \frac{1}{2}, \\ 2\left(1 - \frac{r}{h}\right)^3, & \frac{1}{2} < \frac{r}{h} \leq 1, \\ 0, & \frac{r}{h} > 1. \end{cases} \quad (1)$$

As in Springel et al. (2001) we define the smoothing kernel on the interval  $[0, h]$  and not on  $[0, 2h]$  as frequently done in the literature. The background density at a given halo location is the sum of the contributions of the seven nearest neighbours. Using this recipe, a *background density* is assigned to each host halo which we also address as *environment* of the host. In the subsequent analysis the host halos are ordered according to their background density and average properties of the upper and lower 33% tails are determined separately. We also investigated the outcome based on the upper and lower 20% tails and found very similar results. To improve statistics we choose the larger background density intervals.

## 2.4 The stacking procedure

Besides deriving the average accretion redshift,  $z_{\text{acc}}$ , of the satellite populations as a function of host mass and environment, we aim to study differences in their average dynamical properties. To achieve reasonable statistical significance individual host halos with similar masses and background densities are stacked. For that purpose we subtract the bulk velocity of the host halo from the individual satellite velocities and scale them by the virial velocity of the host,  $V_{\text{vir}}$ . The scaling is done to compensate for the host mass variation within the individual mass bins.

The scaled velocities of satellites belonging to host halos of a given mass at a given background density are used to compute the mean radial velocity,  $v_{\text{rad}}$ , the three dimensional velocity dispersion,  $\sigma_{3\text{D}}$ , its radial and tangential components,  $\sigma_{\text{rad}}$  and  $\sigma_{\text{tan}}$ , and based on these quantities the velocity anisotropy parameter,  $\beta = 1 - 0.5(\sigma_{\text{tan}}^2/\sigma_{\text{rad}}^2)$ . In addition

we compute the average number of satellites,  $N_{\text{sat}}$ , as a function of host mass and environment as well as the average ratio between the actual maximal circular velocity and that one at the time of the satellites' accretion,  $V_{\max}/V_{\max, \text{acc}}$ .

## 3 RESULTS

Before we discuss the environment dependence of accretion times and dynamical structure of satellite systems we review the impact of environment on the host halo properties themselves. Resolution effects are discussed in the final paragraph.

### 3.1 Host halo properties as a function of environment

The left panel of Figure 1 shows the average maximum circular velocity,  $V_{\max}$ , of host halos as a function of mass. Red (solid) and blue (dot-dashed) lines, as with all the remaining figures, show the result for the halos within the upper and lower 33% tails of the background density distributions. Subsequently, we will address the two samples as *high* and *low* density samples. The figure indicates that the average values of  $V_{\max}$  are independent of environment.

The middle panel of Figure 1 displays the concentration,  $c_{\max}$ , as a function of host mass and environment. In agreement with previous studies we find low mass halos with high background densities to be more concentrated compared to their low density counterparts of the same mass. Again, this behaviour is reversed for halo masses above  $\sim 10^{13} h^{-1}M_{\odot}$  (cf., Wechsler et al. 2006; Gao & White 2007; Jing et al. 2007; Macciò et al. 2007; Wetzel et al. 2007; Angulo et al. 2008; Faltenbacher & White 2010).

The right hand panel of Figure 1 depicts the three dimensional velocity dispersion of the host halos,  $\sigma_{3\text{DH}}$ , as a function of mass and environment. Low mass halos in high density regions have higher velocity dispersions compared to their counterparts in low density regions. This behaviour is reversed for higher masses which is similar to what is seen for the concentrations. The analog behaviour of concentration and velocity dispersion is in agreement with predictions based on the Jeans equation (e.g., Faltenbacher & Mathews

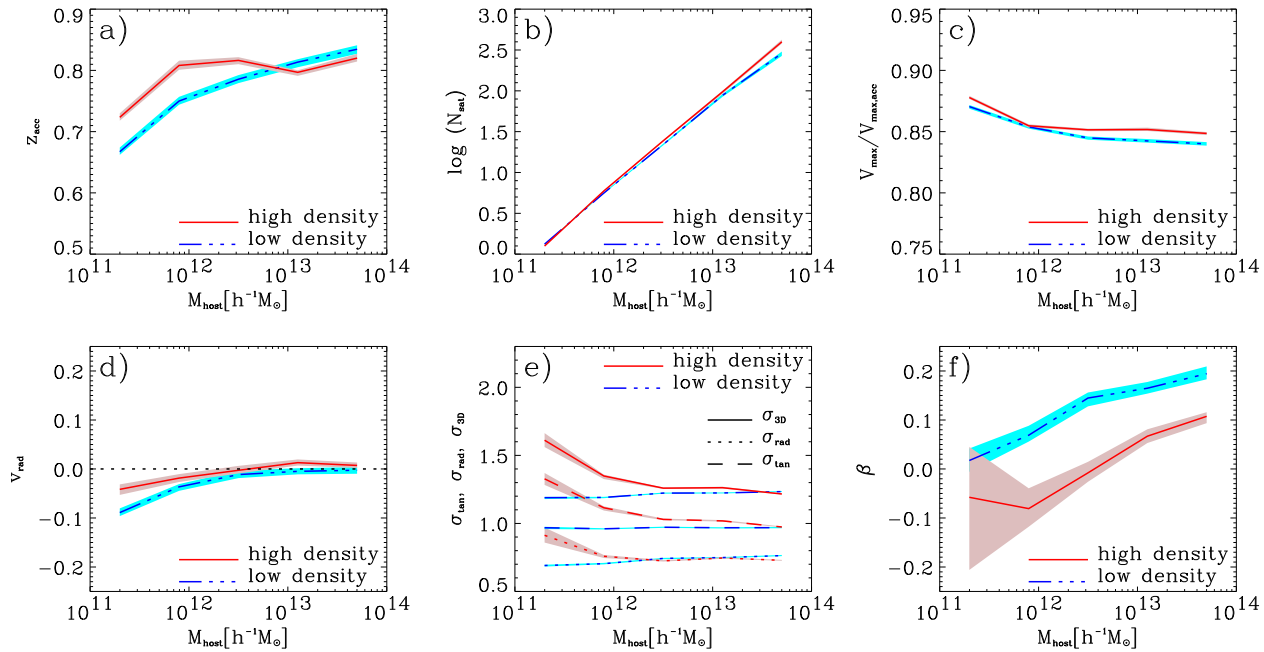


**Figure 2.** Average sub-halo halo properties, redshift of accretion ( $z_{\text{acc}}$ ), number of sub-halos per host halo ( $N_{\text{sat}}$ ), the ratio of the current maximum circular velocity and its values at the time of accretion ( $V_{\text{max}}/V_{\text{max,acc}}$ ), the radial velocity ( $v_{\text{rad}}$ ), the three dimensional velocity dispersion ( $\sigma_{3D}$ ) and the velocity anisotropy  $\beta$  as a function of the host halo mass. Red (solid) and blue (dot-dashed) lines display results based on host halos in the upper and lower 33% tails of their background density distributions. (By analogy, the upper and lower lines of the pairs of dashed and dotted lines correspond to results based on host halos in the upper and lower 33% tails of their background density distributions.) Before averaging the velocity of each individual sub-halo is scaled by the virial velocity of its host halo. The shaded regions indicate the  $1\sigma$  confidence intervals based on a bootstrap resampling.

2007). However, we notice the crossing takes place at some lower masses than seen for the concentrations.

### 3.2 Accretion history and dynamical structure of satellite systems

The upper left panel of Figure 2 displays the average accretion redshift of satellites within host halos at high (red, solid line) and low (blue, dot-dashed line) densities as a function of mass. For hosts below the typical collapse mass,  $M_* = 6.15 \times 10^{12} h^{-1} M_{\odot}$ , satellites in high density regions are accreted earlier compared to satellites in low density regions. For host masses above  $M_*$  the difference becomes marginal or may even reverse. The dependence of satellite accretion times on environment is similar to the observed assembly bias for halos themselves (e.g., Gao et al. 2005). A similar correlation between host halo mass and satellite accretion redshift has also been reported in a study by Lagos et al. (2009). This behaviour can be explained by the fact that as the host mass increases the mean mass of the accreted satellites increases as well and therefore makes the satellite population as a whole more resistant against tidal forces.

At the first glance our findings seem to contradict results by Fakhouri & Ma (2009). They find a modest increase of the merger rates in high density environments at present time. However, the measurement of the mean accretion redshift of surviving satellites is a convolution of the merger rate (over an extended period of time) and the survival rate which may depend on environment as the velocity struc-

ture does. In particular we will see below that satellites in high density environments show a more tangentially biased velocity structure which prevents rapid destruction by the hosts' tidal field as it is the case for more radial orbits. We also checked, whether the satellites' masses at the time of accretion are dependent on environment. It turned out that this is not the case. Therefore, a dependence of the satellite masses on environment can be excluded as explanation of the accretion time differences of the surviving satellite population.

The mean number of satellites for the given host halo masses does not depend on environment as the overlapping graphs in the upper middle panel of Figure 2 indicate. As shown in the upper right panel the average decrease of the maximum circular velocity is about 15% which is slightly reduced for low mass hosts. Consequently, the central profiles of satellite halos remain fairly intact on their orbits within the potential well of the host. This behaviour is in agreement with the study by Kazantzidis et al. (2004), see also Boylan-Kolchin et al. (2009).

The lower left panel of Figure 2 depicts the mean radial velocity of satellites as a function of host mass and environment. All velocities are scaled by the corresponding virial velocity. A radial velocity close to zero indicates that on average the satellite distribution is static which is observed for host halos above  $10^{12} h^{-1} M_{\odot}$ . Negative values correspond to a net infall or some other excess of inward moving satellites.

The lower middle panel in Figure 2 displays the 3D (solid and dot-dashed lines) velocity dispersion of satellites

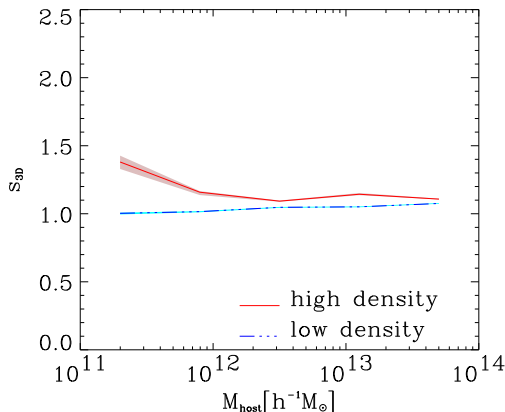


**Figure 3.** Satellite velocity dispersion scaled by the host halo velocity dispersion,  $s_{3D}$ , as a function of host halo mass. Except for the scaling this figure repeats the solid and dot-dashed lines in the velocity dispersion panel of Fig. 2.

and their radial (dotted lines) and the tangential (dashed lines) as a function of host mass and environment. All satellite velocities are computed relative to the bulk velocity of the host halo and scaled by the corresponding virial velocity before averaging. We find a remarkable rise in the dispersions of the satellites in low mass hosts at high densities. These satellites show velocities 30% larger than their counterparts in low density environments. This behaviour is discussed more thoroughly below in the context of Figure 3.

The lower right panel of Figure 2 presents the anisotropy parameter of satellite galaxies as a function of host mass and environment. We find a profound difference in the dynamical structure of satellite systems in high density environments as compared to their counterparts at low background densities ( $\Delta\beta \geq 0.1$ ). Independent of host mass, the satellite velocities in low density environments are more radially biased than those in high density regions. Besides the dependence on environment there is also an obvious trend with host mass. Independent of environment, the velocity structure of satellites is more radially biased within more massive hosts.

Host halos in a low density environments dominate the ambient gravitational field more strongly than their equal mass counterparts at high densities. The gravitational field lines point radially towards the host and so does the acceleration exerted on future satellites. The dynamical structure of the satellites within the host halo is a result of the fairly radial inflow. In contrast, the gravitational field in high density regions is more complex. Before satellites are accreted onto a host they also experience non radial accelerations from other massive haloes nearby. As a result the velocities of satellites show a larger non-radial component. The dependence of  $\beta$  on mass may be interpreted in the same way. The more massive the host the more radial the gravitational acceleration of future satellites. Which results in the more radially biased velocity dispersions of the satellites within high mass hosts.

Figure 3 further explores the large velocity dispersion of satellites in low mass hosts at high background densities.

Here we display the three-dimensional velocity dispersion of the stacked satellite populations scaled by the measured three dimensional velocity dispersions of the host halos and not, as in Figure 2, by the virial velocities. Thus, the velocity dispersion of the satellites are directly compared to that of the host. We find that satellites in host halos at low densities and satellites in high mass hosts (independent of environment) don't show velocity bias. This is in agreement with results in Faltenbacher & Diemand (2006) and Lau et al. (2009). The velocity dispersion of satellites in high density environments deviates from this behaviour. For host masses below  $\sim 10^{12} h^{-1} M_{\odot}$  the satellites are hotter than the overall dark matter component.

This effect can not be explained by more recent accretion times since, in this case, the low density satellites should show even larger dispersions. Recently, Wang et al. (2007) and Fakhouri & Ma (2009) reported on dynamically hotter ambient environments for halos in high density regions. In addition, low mass hosts in dense environments are located next to more massive halos. These halos expel a substantial fraction of their sub-halos out to large radii (e.g., Gill et al. 2004; Ludlow et al. 2009). Thus, satellites which merge onto or pass through the low mass host systems are hotter compared to their counterparts at low densities. It seems plausible that some fraction of satellites within low mass hosts at high densities do originally not belong to the Lagrangean volume of the host halo instead they are accelerated by more massive structures nearby. These satellites are dynamically hotter than the host itself. In the following discussion we address these satellites as *interlopers*.

### 3.3 Abandoning the mass barrier for entering satellites

Figure 4 iterates the analysis presented in Figure 2 with the only difference that the restriction on the maximum circular velocity at the time of accretion,  $V_{\max, \text{acc}} \geq 30 \text{ km s}^{-1}$ , is abandoned. The outcomes presented in this section should not be considered as results per se. They are shown to point out the impact of the  $30 \text{ km s}^{-1}$  restriction. In this case, all satellites which can be detected at present, i.e. all sub-structures which have more than 100 particles at  $z=0$ , contribute to the averaging process. If a sub-halo falls below the 100 particle limit we assume it as tidally *dissolved*. Since many satellites have low masses at the time of accretion tidal dissolution is more prominent in the unrestricted sample. This is the key difference between the satellite sample with and without restriction. In the following we discuss the individual panels in Figure 4 and compare them to the corresponding panels in Figure 2:

- a) The average accretion redshift,  $z_{\text{acc}}$ , is reduced for the unrestricted sample. This is expected since small mass satellites have shorter survival times. Thus, a large fraction of early accreted low mass systems is missing. However, the dependence on environment persists;
- b) The average number of satellites increases by a factor of  $\lesssim 2$ . This is a consequence of the shape of the (sub-)halo mass function (Boylan-Kolchin et al. 2009);
- c) The average fraction between current maximum circular velocity and that at the time of accretion,  $V_{\max}/V_{\max, \text{acc}}$  is increased. This behaviour reflects the low average accretion redshift for the unrestricted satellite sample;

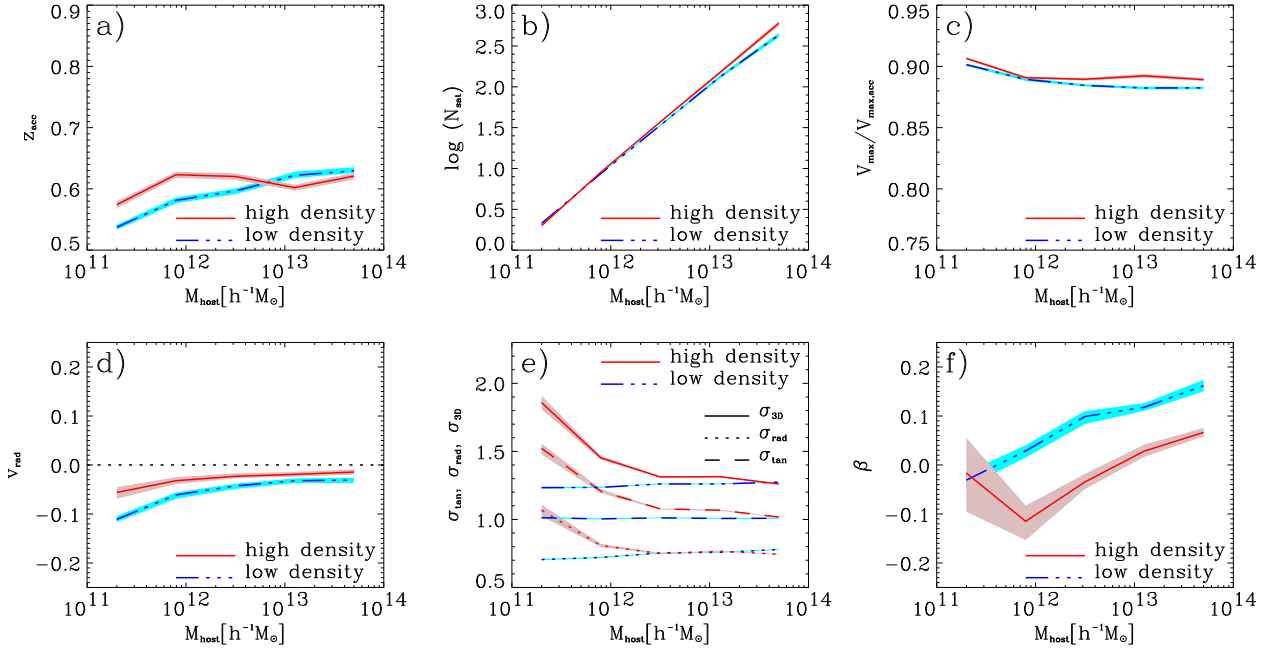


**Figure 4.** Same quantities as in Figure 2 but based on all satellites, i.e. without any restriction on the maximum circular velocity at the time of accretion.

**d)** The average radial velocities,  $v_{\text{rad}}$ , are negative for all host masses. This is a consequence of the lower mass limit of 100 particles for the satellites. As demonstrated in Faltenbacher & Mathews (2007) small mass satellites are most likely to fall below the resolution limit at their pericentre passage causing an excess of negative radial velocities or inward moving satellites;

**e)** The average velocity dispersions,  $\sigma_{3D}$ ,  $\sigma_{\text{rad}}$  and  $\sigma_{\text{tan}}$ , increase by a few per cent, independent of mass and environment. In addition there is a substantial rise in the velocity dispersions of satellites in low mass hosts at high densities. The former effect can be explained by the lower average accretion redshifts. More specifically, the increase of velocity dispersion is a result of the tidal dissolution of earlier accreted satellites which have on average lower velocities. After their dissolution the slow moving satellites do not contribute to the overall dispersion anymore which causes a positive bias of the velocity dispersion. This effect is more noticeable for the satellite sample without restriction of  $V_{\text{max,acc}}$  since there tidal dissolution is more prominent. The increase of the velocity dispersion in low mass systems at high density is presumably an enhanced contribution of low mass interlopers in high density environments;

**f)** The velocity anisotropy parameter,  $\beta$ , decreases by  $\sim 0.05$ , i.e. the tangential velocity component of the satellites is slightly increased for the sample without restriction on  $V_{\text{max,acc}}$ . In addition, we find a distinct upward turn for low mass hosts in dense environments. The former is due to the fact that satellites on more radial orbits penetrate deeper into the potential well of the host. Consequently, they are more strongly exposed to tidal forces and get dissolved faster. The remaining satellite population is biased towards a more prominent tangential velocity component. The upward trend for low mass hosts at high densities may be explained

by interlopers. Dynamically, they are not strongly coupled with the host. Assuming random motions of the interlopers one expects  $\beta = 0$  which, in deed, is nearly approached.

The comparison above highlights the fact that satellites are modelled by dark matter particles of a finite mass ( $6.9 \times 10^6 h^{-1} M_{\odot}$ ) and consequently can not be traced further or are lost when they get tidally striped below a given ‘trustworthy’ mass. Here we set this mass to be  $6.9 \times 10^8 h^{-1} M_{\odot}$  corresponding to 100 particles. Satellites which get tidally striped below this limit ‘disappear’, i.e., they do not contribute to the average values (like accretion redshift, velocity dispersion etc.) for the satellite populations anymore. This causes a bias towards later accreted satellites and the consecutive effects. In particular the large number of approaching satellites with masses only slightly above the mass cut contributes to that bias. However, if the restriction  $V_{\text{max,acc}} \geq 30 \text{ km s}^{-1}$  is imposed these effects are not apparent. In that case the satellites comprise on average a few 1000 particles at the time of accretion. Even substantial tidal stripping does not push the satellite below the lower particle limit, i.e. all arriving satellites have extended survival times. Therefore, the results presented in Figure 2 describe physical phenomena and are not caused by the finite masses of the simulation particles.

## 4 CONCLUSION

Taking advantage of the superior resolution of the Millennium–II Simulation we determine the impact of assembly bias on galaxy systems. We conclude with a recapitulation of the main results:

1) The average accretion redshift depends on the host mass and environment. For host masses of  $10^{11} h^{-1} M_{\odot}$  we find  $z_{\text{acc}} \approx 0.7$  which increases for host halos above  $10^{13} h^{-1} M_{\odot}$



to  $z_{\text{acc}} \approx 0.8$ . The average accretion redshift of satellite halos in high density environments is larger,  $\Delta z \approx 0.1$ , compared to that of their counterparts in low density regions. The dependence of satellite accretion times on environment is most likely caused by the more tangentially biased velocity structure (see point 3) of satellites in high density regions which makes them more resistant to the hosts' tidal field. In contrast satellites in low density environments show more radially biased velocity structures. As a consequence total tidal dissolution of these satellites may happen faster causing a lower average accretion redshift of the surviving satellite population.

2) Host halos above  $10^{12} h^{-1} M_{\odot}$  show the same velocity dispersion as their satellite populations. This remains valid for lower mass halos in low density environments. However, the dispersion of satellites within low mass hosts at high densities exceed that of the hosts by  $\sim 30\%$ . Which may be interpreted as contamination by high velocity interlopers.

3) The velocity anisotropy of satellite halos is correlated with the mass of the host halo. More massive hosts show more radially biased satellite velocities. In addition we find a strong dependence of the velocity anisotropy on environment. Satellite velocities of host halos residing in high density environments tend to be less radially biased than those in low density environments.

Our findings show that the internal dynamical structure of satellite systems is correlated with environment. We believe that our approach allows to make similar predictions for real satellite galaxy systems. Thus the dynamical structure of satellite galaxy systems should depend on environment. Most notably satellites of host galaxies in less dense environments show a more radially biased velocity structure. This behaviour may have implications for the accretion process of the host galaxies.

## ACKNOWLEDGEMENTS

We would like to thank the anonymous referee for useful remarks, Simon White and Mike Boylan-Kolchin for insightful comments and Russell Johnston for careful revisions which helped to improve the paper. It is a pleasure to acknowledge the South African Astronomical Observatory or kind hospitality. The Millennium-II Simulation databases used in this paper and the web application providing online access to them were constructed as part of the activities of the German Astrophysical Virtual Observatory. Data for halos and galaxies are publicly available at <http://www.mpa-garching.mpg.de/millennium>.

## REFERENCES

Angulo R. E., Baugh C. M., Lacey C. G., 2008, MNRAS, 387, 921  
 Bett P., Eke V., Frenk C. S., Jenkins A., Helly J., Navarro J., 2007, MNRAS, 376, 215  
 Bond J. R., Cole S., Efstathiou G., Kaiser N., 1991, ApJ, 379, 440  
 Boylan-Kolchin M., Springel V., White S. D. M., Jenkins A., 2009, ArXiv e-prints, 0911.4484

Boylan-Kolchin M., Springel V., White S. D. M., Jenkins A., Lemson G., 2009, MNRAS, 398, 1150  
 Cole S., Kaiser N., 1989, MNRAS, 237, 1127  
 Dalal N., White M., Bond J. R., Shirokov A., 2008, ApJ, 687, 12  
 Fakhouri O., Ma C., 2009, MNRAS, 394, 1825  
 Fakhouri O., Ma C., 2010, MNRAS, 401, 2245  
 Faltenbacher A., Diemand J., 2006, MNRAS, 369, 1698  
 Faltenbacher A., Mathews W. G., 2007, MNRAS, 375, 313  
 Faltenbacher A., White S. D. M., 2010, ApJ, 708, 469  
 Gao L., Springel V., White S. D. M., 2005, MNRAS, 363, L66  
 Gao L., White S. D. M., 2007, MNRAS, 377, L5  
 Gill S. P. D., Knebe A., Gibson B. K., Dopita M. A., 2004, MNRAS, 351, 410  
 Gottlöber S., Kerscher M., Kravtsov A. V., Faltenbacher A., Klypin A., Müller V., 2002, A&A, 387, 778  
 Gottlöber S., Klypin A., Kravtsov A. V., 2001, Progress in Astronomy, 19, 58  
 Guo Q., White S., Li C., Boylan-Kolchin M., 2010, MNRAS, pp 367–+  
 Hahn O., Porciani C., Carollo C. M., Dekel A., 2007, MNRAS, 375, 489  
 Hahn O., Porciani C., Dekel A., Carollo C. M., 2009, MNRAS, 398, 1742  
 Harker G., Cole S., Helly J., Frenk C., Jenkins A., 2006, MNRAS, 367, 1039  
 Jing Y. P., Suto Y., Mo H. J., 2007, ApJ, 657, 664  
 Kaiser N., 1984, ApJ, 284, L9  
 Kazantzidis S., Mayer L., Mastropietro C., Diemand J., Stadel J., Moore B., 2004, ApJ, 608, 663  
 Kravtsov A. V., Gnedin O. Y., Klypin A. A., 2004, ApJ, 609, 482  
 Lacey C., Cole S., 1993, MNRAS, 262, 627  
 Lagos C. D. P., Padilla N. D., Cora S. A., 2009, MNRAS, 397, L31  
 Lau E. T., Kravtsov A. V., Nagai D., 2009, ApJ, 705, 1129  
 Ludlow A. D., Navarro J. F., Springel V., Jenkins A., Frenk C. S., Helmi A., 2009, ApJ, 692, 931  
 Macciò A. V., Dutton A. A., van den Bosch F. C., Moore B., Potter D., Stadel J., 2007, MNRAS, 378, 55  
 Mo H. J., White S. D. M., 1996, MNRAS, 282, 347  
 Monaghan J. J., Lattanzio J. C., 1985, A&A, 149, 135  
 Navarro J. F., Frenk C. S., White S. D. M., 1997, ApJ, 490, 493  
 Press W. H., Schechter P., 1974, ApJ, 187, 425  
 Sheth R. K., Tormen G., 2004, MNRAS, 350, 1385  
 Springel V., 2005, MNRAS, 364, 1105  
 Springel V., White S. D. M., Tormen G., Kauffmann G., 2001, MNRAS, 328, 726  
 Springel V., Yoshida N., White S. D. M., 2001, New Astronomy, 6, 79  
 Wang H. Y., Mo H. J., Jing Y. P., 2007, MNRAS, 375, 633  
 Wechsler R. H., Bullock J. S., Primack J. R., Kravtsov A. V., Dekel A., 2002, ApJ, 568, 52  
 Wechsler R. H., Zentner A. R., Bullock J. S., Kravtsov A. V., Allgood B., 2006, ApJ, 652, 71  
 Wetzel A. R., Cohn J. D., White M., Holz D. E., Warren M. S., 2007, ApJ, 656, 139  
 Zentner A. R., 2007, International Journal of Modern Physics D, 16, 763